V−doped T−Nb_2O_5 toward high−performance Mg^{2+}/Li^+ hybrid ion batteries

Huihuang Huang,[a] Guangyu Zhao,*[ab] Xianbo Yu,[a] Xiaojie Shen,[a] Ming Wang,[a] Xiaoming Bai[a] and Naiqing Zhang*[ab]

[a] State Key Laboratory of Urban Water Resource and Environment, School of Chemistry and Chemical Engineering, Harbin Institute of Technology, Harbin 150001, China.
[b] Academy of Fundamental and Interdisciplinary Sciences, Harbin Institute of Technology, Harbin 150001, China. E-mail: zhaogy810525@gmail.com; znqmww@163.com.

Experimental section

All the chemical reagents were analytical grade and obtained commercially.

Synthesis of materials

The V−doped T−Nb_2O_5 were synthesized via a facile solvothermal reaction and heating treatment. The niobium pentachloride ($NbCl_5$, 99.9%, Aladdin), Vanadyl acetylacetonate (98%, Aladdin) and Tetramethylammonium hydroxide aqueous (TMAOH, 1 M, Aladdin) were used as starting materials. By changing the amount of Vanadyl acetylacetonate ($VO(acac)_2$, 0, 0.05, 0.1, 0.15 mmol), the various V−doped T−Nb_2O_5 were prepared. The final products were denoted as TNO, VTNO−1, VTNO−2 and VTNO−3, respectively. Briefly, 5 mmol of $NbCl_5$ and a certain amount of $VO(acac)_2$ (0, 0.05, 0.1, 0.15 mmol) were dissolved in 70 mL of ethanol under continuous stirring for 30 min, then 1.5 mL of TMAOH was added to above solution and stirred for 2 h. And the aforementioned mixtures were transferred to 100 mL Teflon−lined autoclave. Afterwards, the autoclave was sealed and kept at 200 ℃ for 20 h. The obtained products were washed with ethanol and water several times and dried at 80 ℃ in vacuum. Finally, the V−doped T−Nb_2O_5 were obtained by heating treated at 700 ℃ for 3 h under Ar atmosphere.

Preparation of electrolytes

All the operations were operated in an argon−filled glove box (< 0.1 ppm of water and oxygen) at room temperature. The APC electrolyte for MRB was prepared according to reported literature. Firstly, 1.067 g of aluminum chloride was slowly dissolved in 12 mL of Tetrahydrofuran (THF) under vigorous stirring and kept for 12 h. Subsequently, the transparent solution was added to 8 mL phenyl magnesium chloride (2 M in THF) dropwise under continuous stirring and kept for another 12 h to obtain the 0.4 M APC electrolyte. Finally, 0.848 g of anhydrous LiCl was dissolved in APC electrolyte to obtain 0.4 M APC–1.0 M LiCl electrolyte for MLIB.

Material characterization

The morphology and microstructure of products were conducted by Field emission scanning electron microscope (SEM, Hitachi, SU8010) with energy dispersive spectrometer (EDS) mapping and transmission electron microscope (TEM, JEM–2100 with an accelerating voltage of 200 kV). The X−ray diffraction (XRD) patterns of materials were characterized by PANalytical X'Pert PRO with Cu Kα radiation (λ =1.5418 Å). The X−ray photoelectron spectroscopy (XPS) were obtained by a K−Alpha electron spectrometer (Thermo Fischer Scientific Company) using Al Ka (1486.6 eV) radiation. The binding energies were referenced to the C 1s line at 284.8 eV from adventitious carbon. The Raman spectra of products were performed with 532 nm laser radiation. The ultraviolet−visible diffuse reflectance spectra (UV−Vis DRS) of samples were recorded on a Shimadzu UV−2600 spectrophotometer. The BET surface area and pore size distribution were characterized by the Micromeritics ASAP 2020.

Electrochemical characterization

All the electrochemical performances of samples were evaluated with 2025−type coin cell which were assembled in an argon−filled glove box, using as−synthesized products as cathodes, Mg foil as the reference and counter electrodes and Microporous membrane (Celgard 2400) was employed as the separator. The working electrode slurry was prepared by mixing active materials, acetylene black and poly−vinylidene fluoride

(PVDF) binder in a weight ratio of 8:1:1 and N−methyl−2−pyrrolidone (NMP) as solvent. The slurry was pasted on the carbon fiber paper and dried at 80 ℃ in a vacuum oven overnight. For ex-situ XRD analysis, Mo foil as the current collector. 0.4 M APC/THF and 0.4 M APC−1.0 M LiCl/THF were employed as the electrolyte of MRB and MLIB, respectively. Galvanostatic charge/discharge measurements were performed at ambient temperature by a battery test system (Shenzhen Neware Electronic Co., China) from 0.2−2.0 V vs Mg^{2+}/Mg. Cyclic voltammetry (CV) measurements were investigated by CHI 660D electrochemical workstation. Electrochemical impedance spectroscopy (EIS) measurements were conducted with Princeton Applied Research PARSTAT 2273 advanced electrochemical system with 5 mV amplitude, and the frequency range between 100 kHz and 0.1 Hz at open circuit potential.

Galvanostatic intermittent titration technique (GITT) was tested by a battery test system (Shenzhen Neware Electronic Co., China). GITT was conducted with a constant current pulse time of 15 min followed by a relaxation process of 60 min at a current density of 80 mA g^{-1}. The diffusion coefficient can be calculated by the following equation:[1]

$$D = \frac{4}{\pi\tau}\left(\frac{m_B V_M}{M_B S}\right)^2\left(\frac{\Delta E_s}{\Delta E_t}\right)^2 \quad (1)$$

where τ represents the time of current pulse. m_B, V_M and M_B correspond to the mass, molar volume and molar mass of active materials, respectively. S is the contact area of electrode−electrolyte. ΔE_s and ΔE_t represent the potential change caused by the current pulse and potential change during the constant current charge/discharge.

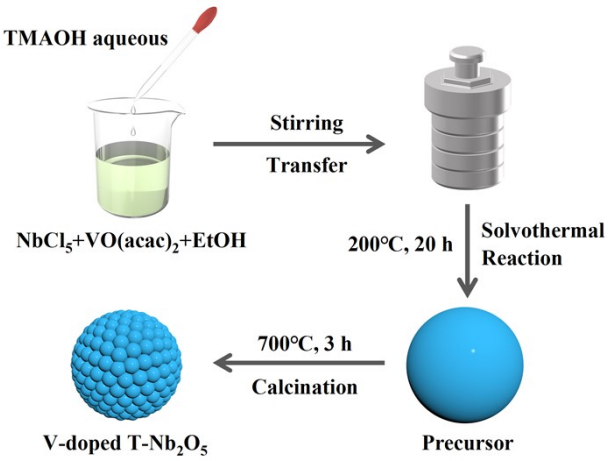

Figure S1. Diagrammatic sketch of the synthetic process of V−doped T−Nb_2O_5.

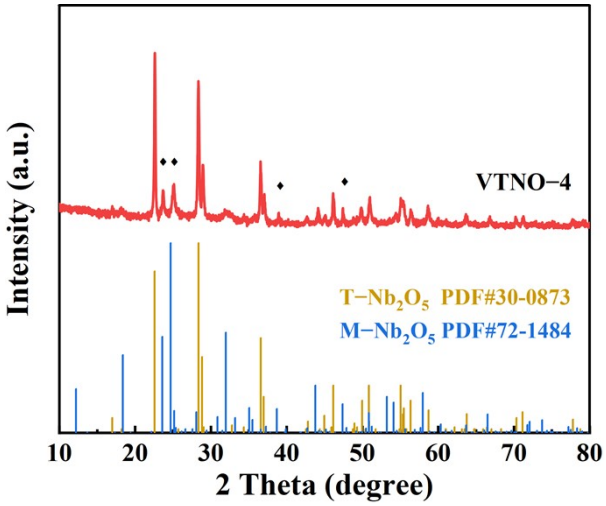

Figure S2. XRD pattern of VTNO−4.

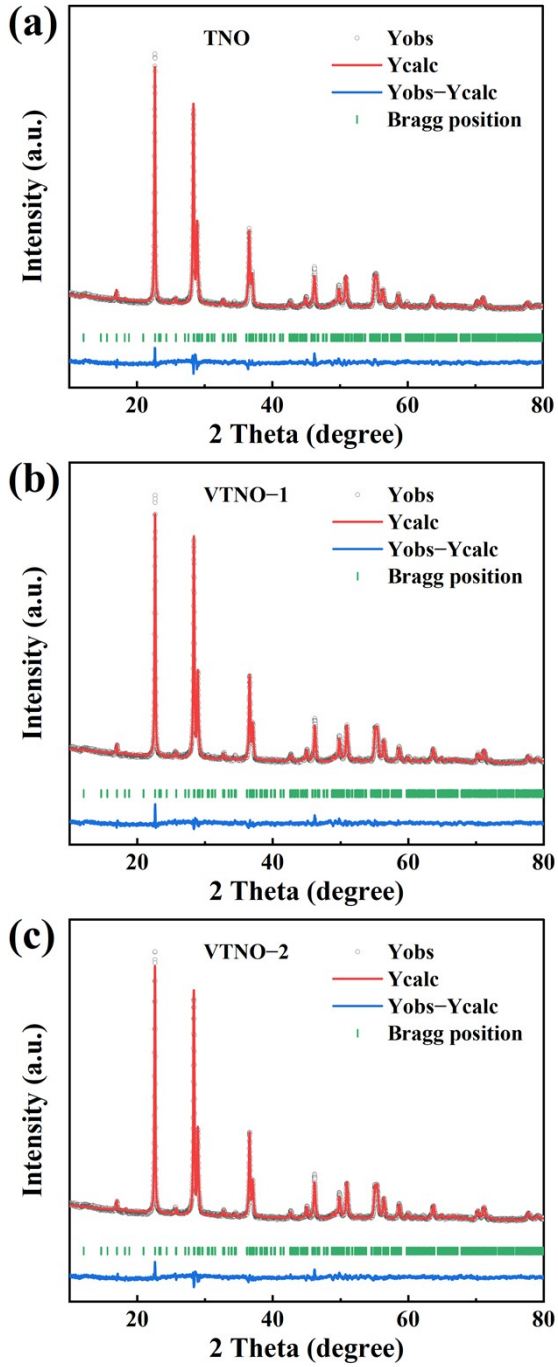

Figure S3. The Rietveld refinement of XRD patterns. (a) TNO, (b) VTNO−1, (c)VTNO−2.

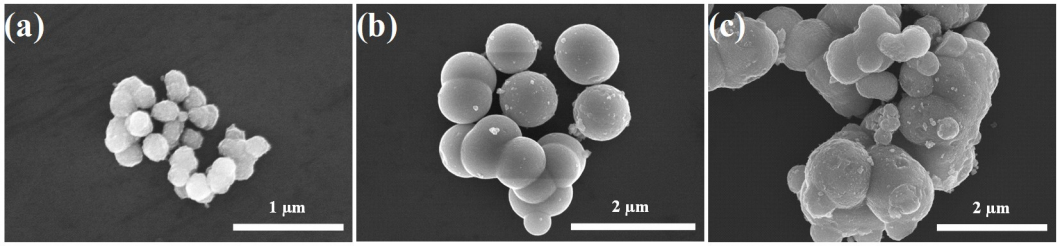

Figure S4. SEM images of the precursors obtained from different concentrations of tetramethylammonium hydroxide. (a) 0.5 M, (b) 1.0 M, (c) 2.0 M.

Figure S4 shows the SEM images of precursors obtained from different concentrations of tetramethylammonium hydroxide (TMAOH, 0.5 M, 1.0 M and 2.0 M) during the synthetic process. The precursor prepared by a low concentration of 0.5 M shows a morphology of spheres with average diameter of about 200 nm. As the concentration rising to 1.0 M, the diameter of spheres increases to around 800 nm. When the concentration is 2.0 M, it is obvious that the agglomeration of spherical structure is serious and the particle size is uneven. Considering the good dispersibility and the micro-nano hierarchical structure, 1.0 M is selected as the optimal concentration.

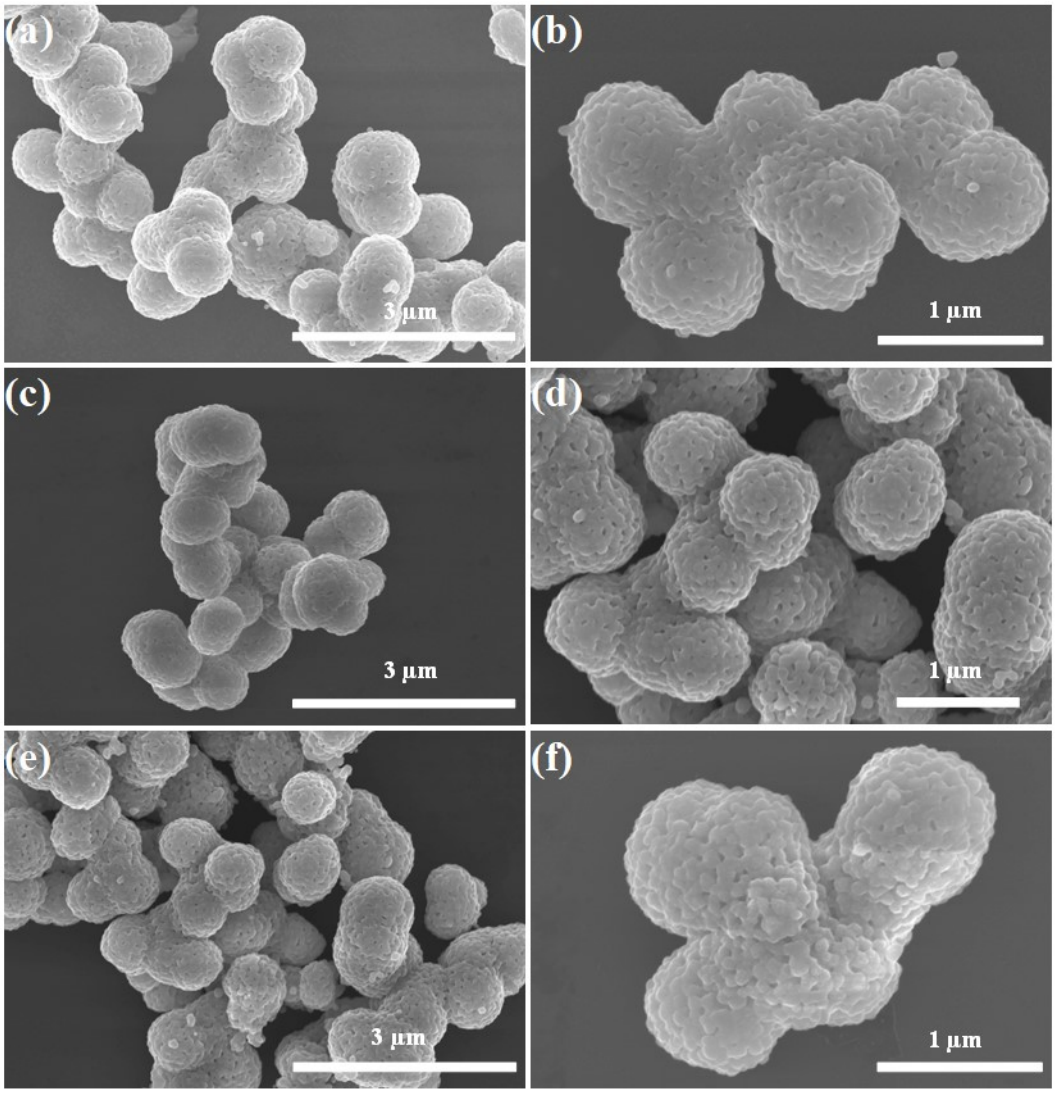

Figure S5. The SEM images of (a, b) TNO, (c, d) VTNO−1 and (e, f) VTNO−2.

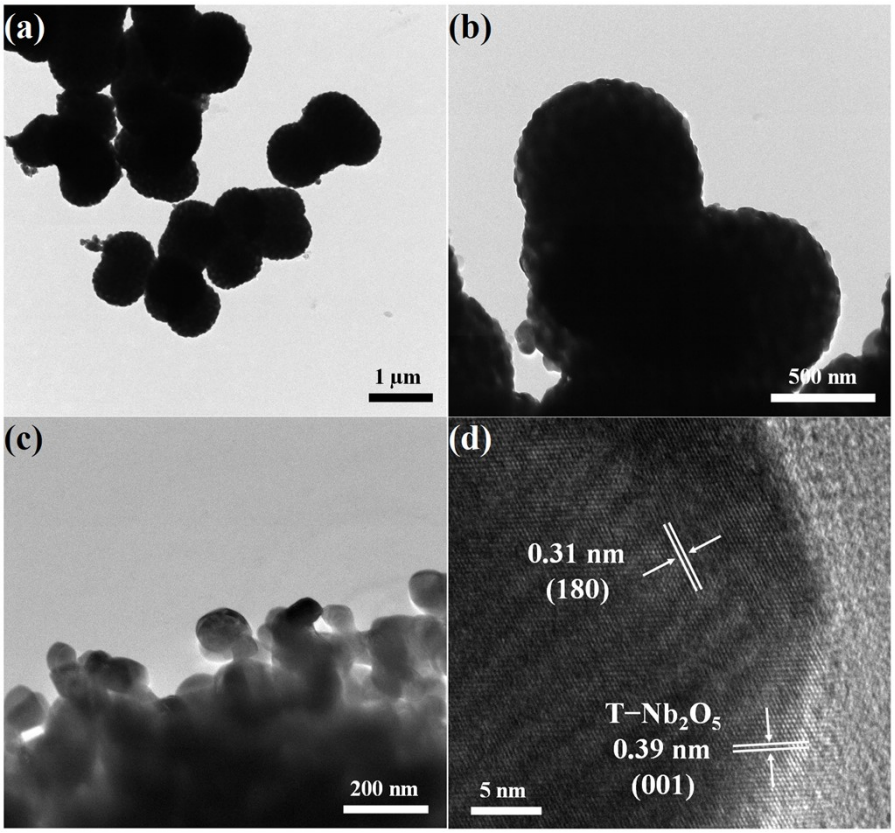

Figure S6. (a−c) TEM images and (d) HR−TEM image[2] of TNO.

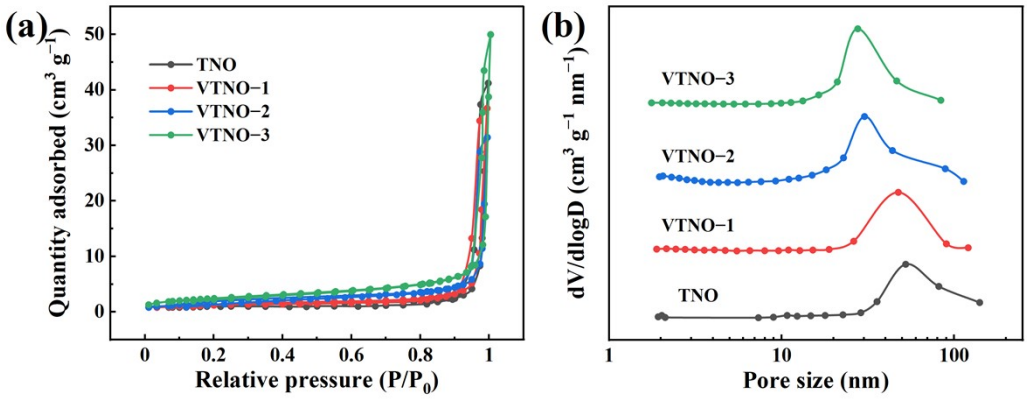

Figure S7. (a)The nitrogen adsorption–desorption isotherms and corresponding (b) pore size distribution.

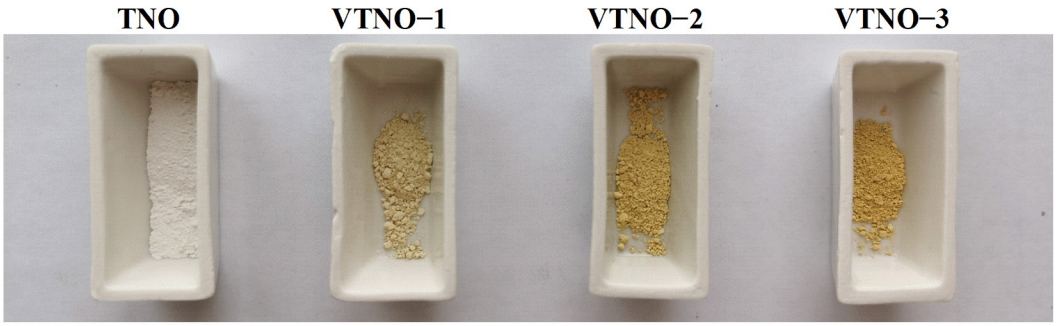

Figure S8. The optical photographs of TNO and VTNO−x (x = 1, 2, 3).

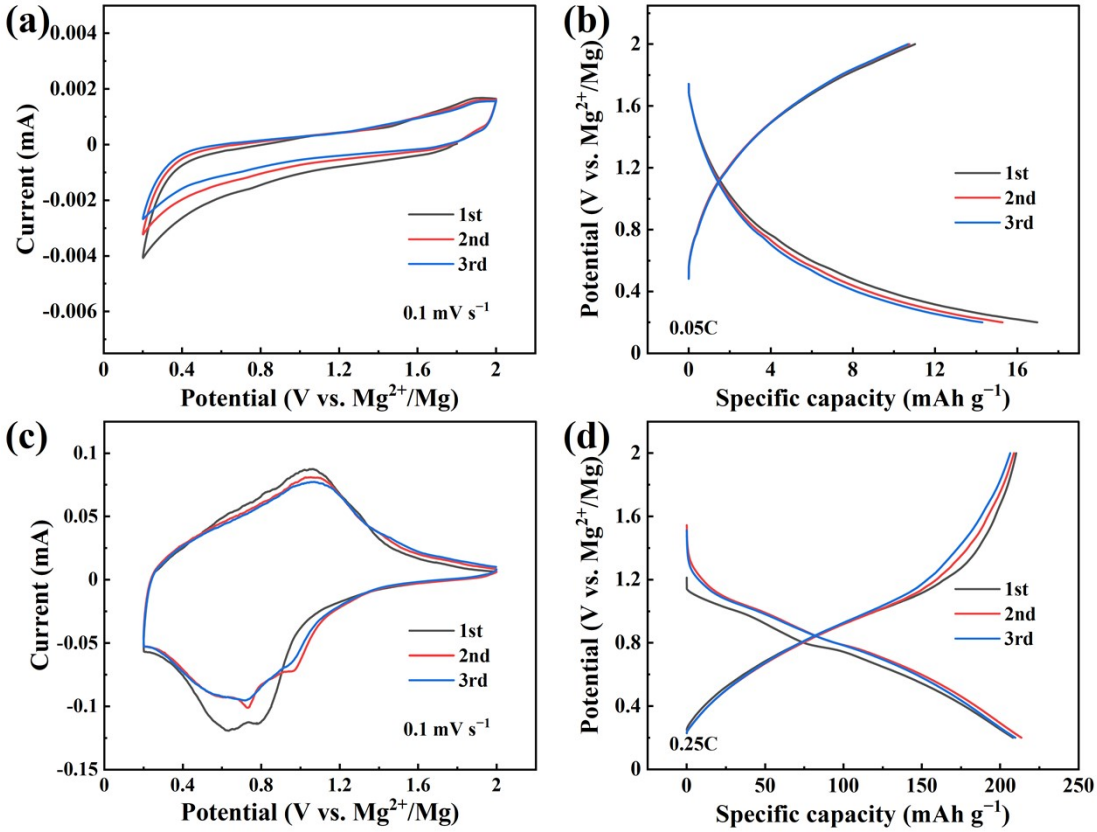

Figure S9. The CV curves of VTNO−3 in (a) MRB and (c) MLIB. The galvanostatic charge/discharge curves of VTNO−3 in (b) MRB and (d) MLIB.

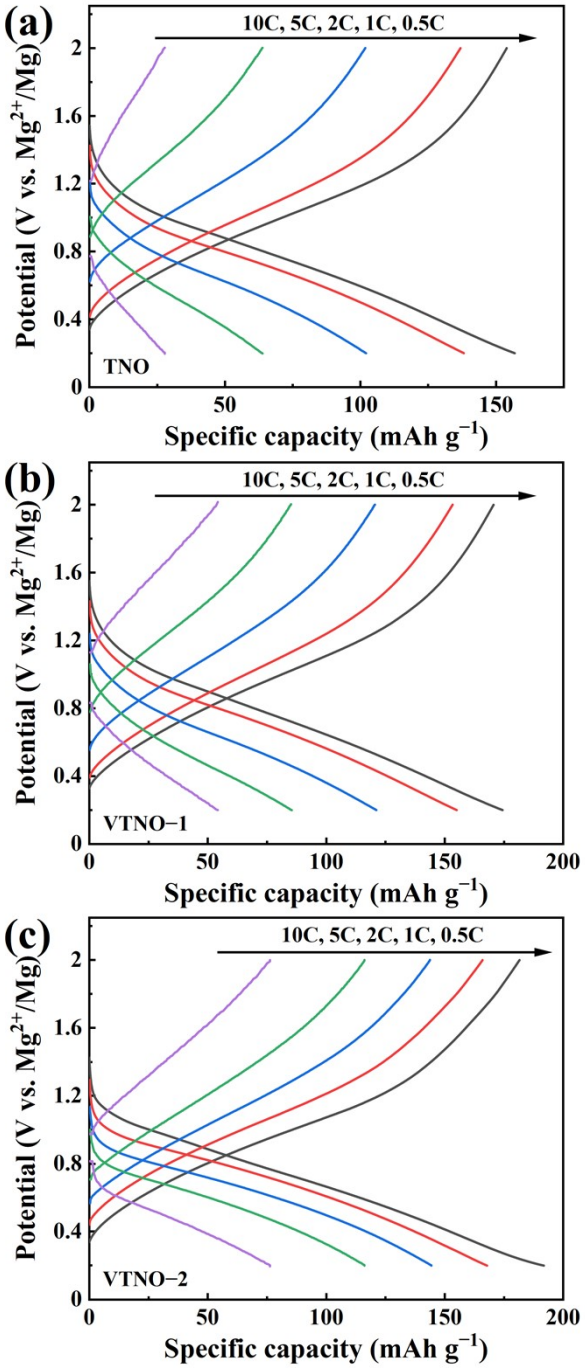

Figure S10. The galvanostatic charge/discharge curves at various current densities. (a) TNO, (b) VTNO−1 and (c) VTNO−2.

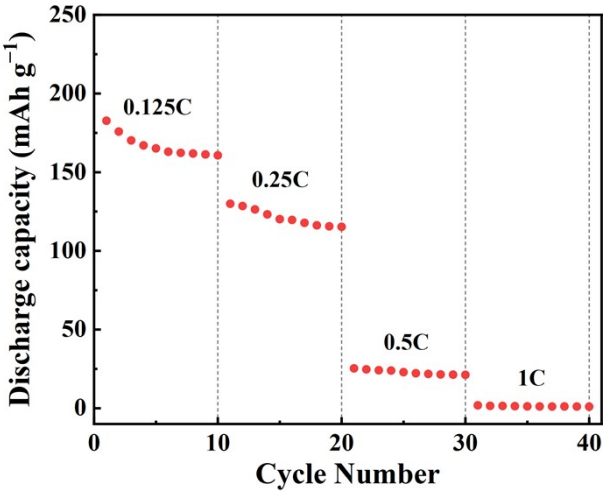

Figure S11. Rate performance of VTNO−3 in pure Li^+ electrolyte.

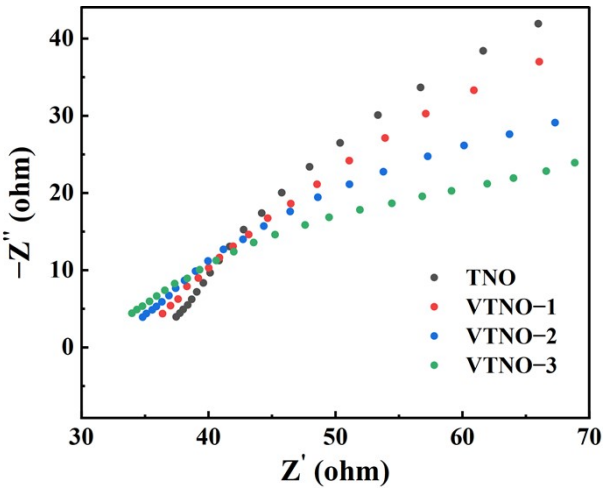

Figure S12. The enlarged Nyquist plots of TNO and VTNO−x (x = 1, 2, 3).

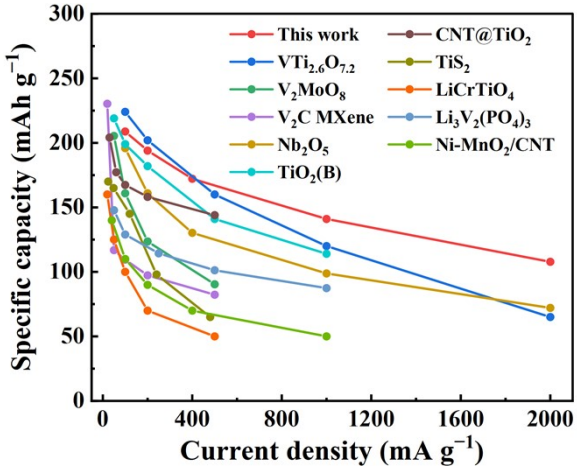

Figure S13. The rate performance of VTNO−3 compares with other reported advanced electrode materials in MLIB.

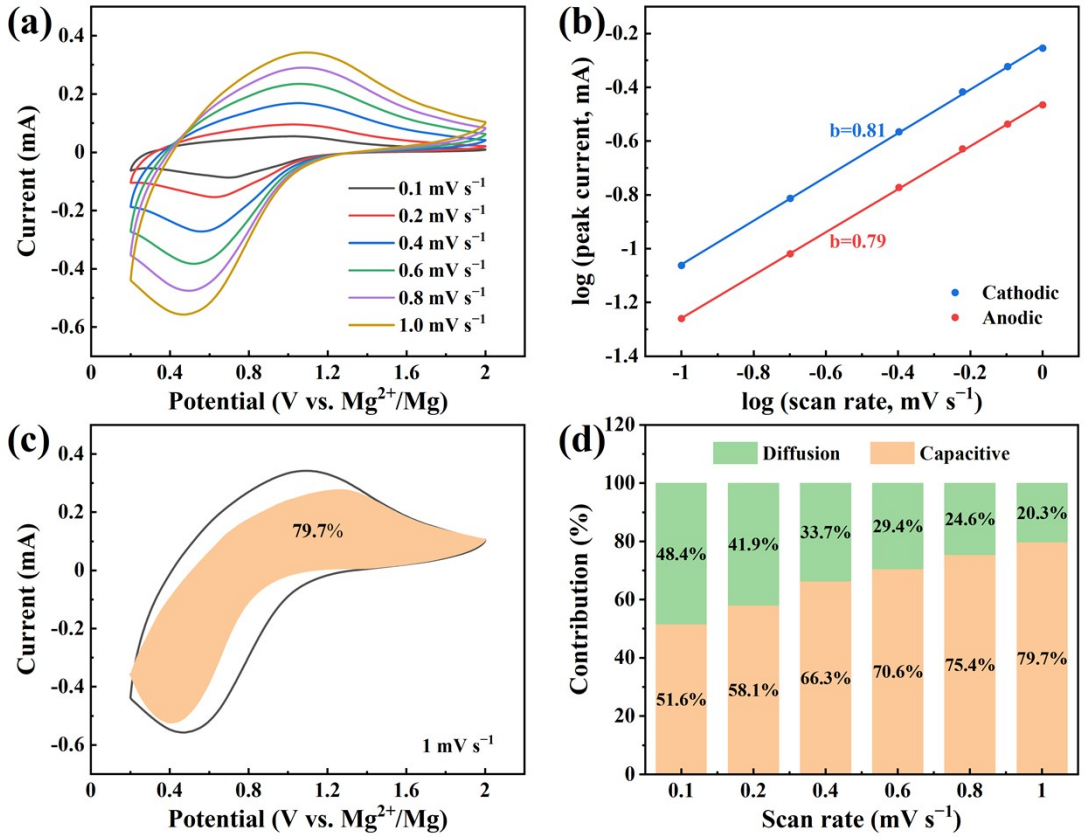

Figure S14. The experimental analyses of electrochemical kinetics for TNO in MLIB: (a) CV curves at various scan rates, (b) the relationship between log (scan rate) and log (peak current) based on the CV curves at redox peaks, (c) the capacitive contribution at 1.0 mV s^{-1}, (d) corresponding capacitive and diffusion contributions at various scan rates.

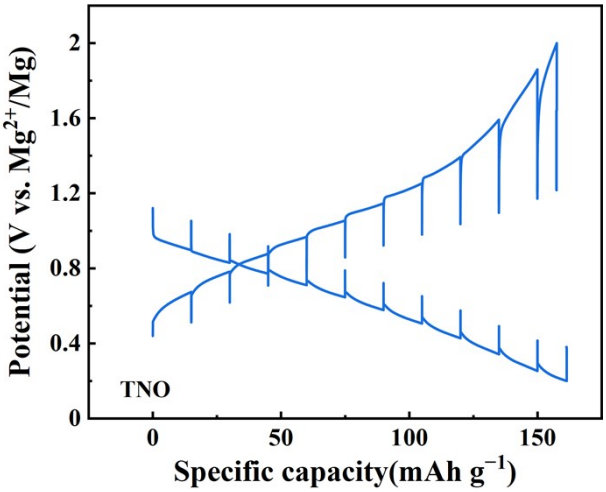

Figure S15. The GITT profile of TNO.

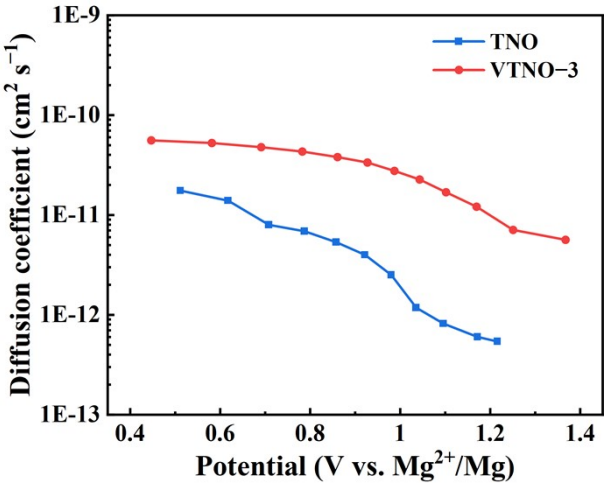

Figure S16. The D−value of TNO and VTNO−3 during the charge process.

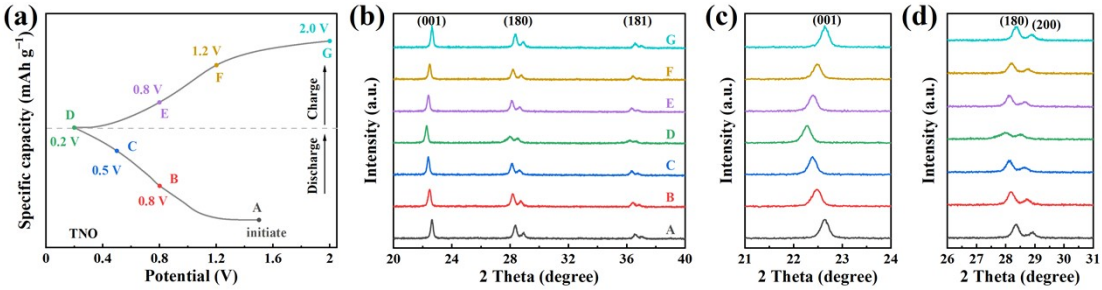

Figure S17. Ex−situ XRD analysis of TNO at diverse charge−discharge states and magnified XRD patterns of (001) and (180) diffraction peaks.

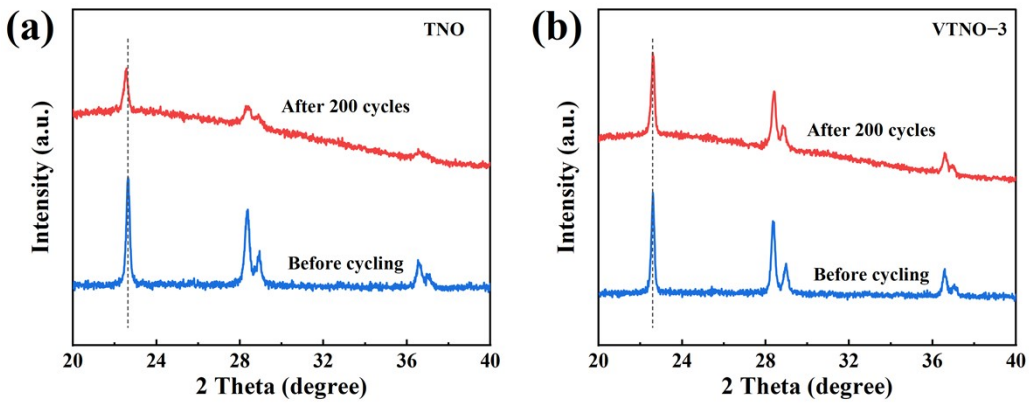

Figure S18. XRD patterns of TNO and VTNO−3 before and after 200 cycles at 1C.

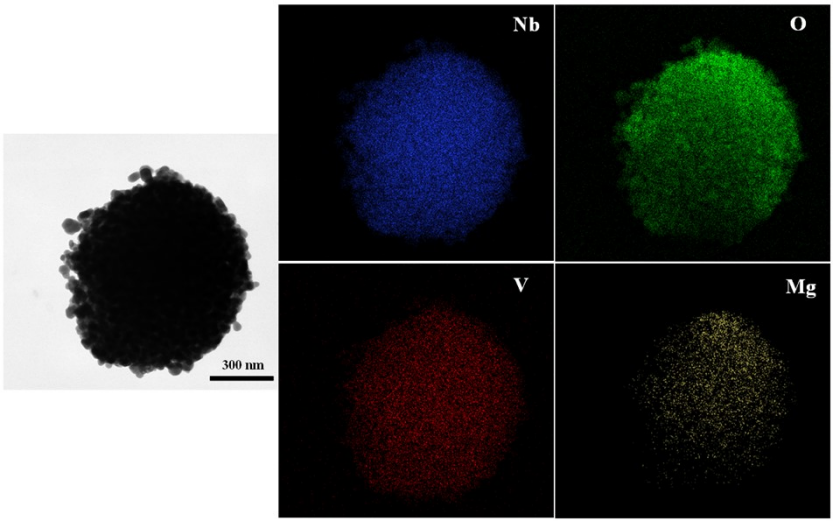

Figure S19. TEM image and corresponding EDS mapping images of VTNO−3 after discharging.

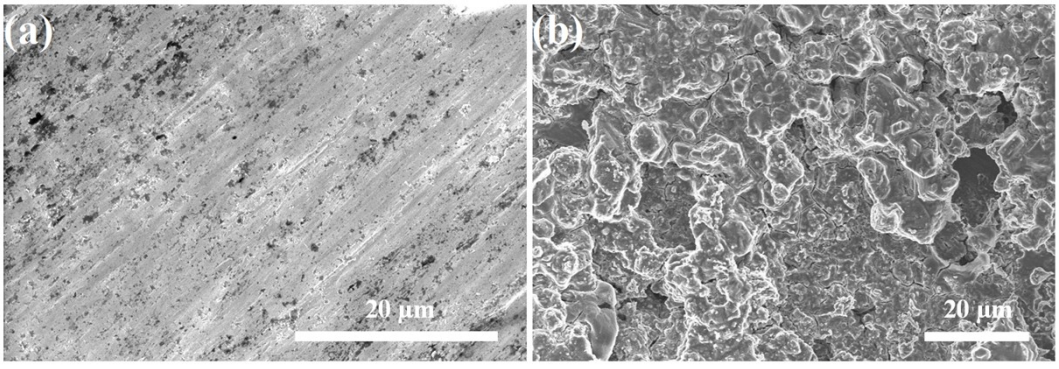

Figure S20. SEM images of Mg metal anode (a) before and (b) after 200 cycles at 1C.

Table S1. The summary of refinement parameters for all samples

	TNO	VTNO−1	VTNO−2	VTNO−3
Space group		Pbam		
Crystal system		Orthorhombic		
α/°		90		
β/°		90		
γ/°		90		
a/Å	6.1790	6.1740	6.1689	6.1659
b/Å	29.2683	29.2674	29.2636	29.2587
c/Å	3.9260	3.9277	3.9307	3.9326
V/Å^3	710.01	709.72	709.59	709.46
R_p/%	3.49	3.31	3.41	3.58
R_{wp}/%	4.38	4.14	4.24	4.46

Table S2. The molar ratio of V: Nb obtained from EDS and ICP−OES.

	EDS (V: Nb, %)	ICP −OES (V: Nb, %)
TNO	0	0
VTNO−1	0.87	0.93
VTNO−2	1.69	1.88
VTNO−3	2.43	2.75

Table S3. The summary of surface area, pore size and band gap for all samples

	Surface area ($m^2\ g^{-1}$)	Pore size (nm)	Band gap (eV)
TNO	5.2	52.4	3.24
VTNO−1	6.3	47.4	3.14
VTNO−2	7.9	30.2	3.06
VTNO−3	9.2	27.6	3.02

Table **S4.** Comparison of cycling stability of VTNO−3 with other reported advanced electrode materials for MLIB.

Materials	**Current Density (mA g^{-1})**	**Reversible Capacity (mA h g^{-1})**	**Cycle Number (n)**	**Retention**	**Reference**
V−doped T−Nb_2O_5 (VTNO−3)	200 1000	181.6 119.3	200 5000	90.5% 82.2%	This work
V_2MoO_8	20	135.8	50	72.5%	*Nano Energy*, 2017, 34, 26
CNT@TiO_2	30	161.9	100	69.3%	*J. Colloid Interface Sci.*, 2021, 581, 307
MoS_2−CuS−EG	50	172.4	200	47.4%	*Chem. Eng. J.*, 2021, 409, 128271
$Li_3V_2(PO_4)_3$	100	127.4	200	75.0%	*J. Mater. Chem. A*, 2019, 7, 9968
$Cu_{1.96}S$−MoS_2−MoO_2	100	150.0	200	68.2%	*ACS Appl. Mater. Interfaces*, 2019, 11, 5966
$K_2C_6O_6$	435	130.0	500	65.0%	*Energy Storage Mater.*, 2019, 22, 218
$VTi_{2.6}O_{7.2}$	1000	122.2	1200	84.2%	*J. Mater. Chem. A*, 2018, 6, 13901.
MoS_2/G VH	1000	145.8	2200	70.0%	*Adv. Funct. Mater.* 2021, 2103214.
VS_4	1000	110.0	1500	52.0%	*Energy Storage Mater.*, 2019, 23, 741.
T−Nb_2O_5 holey nanosheet	200 1000	139.8 65.9	100 400	70.0% 65.9%	*Nanoscale*, 2019, 11, 16222

References

1. P.−F. Wang, T. Jin, J. Zhang, Q.−C. Wang, X. Ji, C. Cui, N. Piao, S. Liu, J. Xu, X.−Q. Yang and C. Wang, *Nano Energy*, 2020, **77**, 105167.